

Electronic structure of rhombohedral CrX₃ (X = Br, Cl, I) van der Waals crystalsL. Craco,^{1,2} S. S. Carara,¹ Y.-C. Shao,^{3,4} Y.-D. Chuang,³ and B. Freelon^{4,5}¹*Institute of Physics, Federal University of Mato Grosso, 78060-900 Cuiabá, MT, Brazil*²*Leibniz Institute for Solid State and Materials Research Dresden, D-01069 Dresden, Germany*³*Advanced Light Source, Lawrence Berkeley National Laboratory, Berkeley, California 94720, USA*⁴*Department of Physics, University of Houston, Houston, Texas 77204, USA*⁵*Texas Center for Superconductivity, University of Houston, Houston, Texas 77204, USA*

(Received 17 February 2021; revised 22 April 2021; accepted 1 June 2021; published 10 June 2021)

We perform a comprehensive analysis of both the chemical and correlated electronic structure reconstruction of rhombohedral CrX₃ (X = Br, Cl, I) van der Waals bulk crystals. Using the generalized gradient approximation (GGA) plus dynamical mean-field theory we explicitly demonstrate the importance of local dynamical correlations for a consistent understanding of emergent Kondo quasiparticles and Mott localized electronic states, showing the interplay between material-dependent one-electron GGA line-shape and multiorbital electronic interactions. To probe the correlated paramagnetic electronic state we performed x-ray absorption spectroscopy measurements for CrCl₃ and CrBr₃ bulk crystals. Our correlated many-body study is relevant to understanding the electronic structure reconstruction of paramagnetic Cr-trihalide crystals and should be widely applicable to other van der Waals magnetic materials.

DOI: [10.1103/PhysRevB.103.235119](https://doi.org/10.1103/PhysRevB.103.235119)**I. INTRODUCTION**

Layered van der Waals chromium trihalide [CrX₃ (X = Br, Cl, I)] compounds have received growing interest in recent years [1–4] due to their extraordinary electronic and magnetic properties [5–14] as well as the opportunity for the development of future functional heterostructures [15,16]. In each layer, Cr and X atoms are arranged in a hexagonal network, in which one Cr atom is bonded to its six neighboring X atoms to form edge-shared octahedra. The resulting Cr-X layers are stacked along the *c* axis and held by van der Waals interactions [16]. All CrX₃ crystals are paramagnetic at room temperature, but their magnetism shows different ground state properties at low temperatures: Both CrI₃ and CrBr₃ bulk crystals are ferromagnetic with Curie temperatures (*T_C*) of 61 K [5] and 37 K [8], respectively, whereas CrCl₃ is antiferromagnetic with a Néel temperature of 16.8 K [9]. Interestingly, structural phase transitions from the rhombohedral to monoclinic symmetry are also observed at different temperatures, i.e., 210 K for CrI₃, 230 K for CrCl₃, and 420 K for CrBr₃ [5,7]. These transitions do not involve any magnetic changes. However, some observed anomalies in the magnetic susceptibility at the crystallographic phase transition of CrCl₃ [5] as well as in the lattice spacing at *T_C* of CrI₃ indicate the coupling between lattice and spin degrees of freedom [14]. Particularly interesting in this regard is CrI₃, which shows a layer-dependent magnetic ground state [17,18]. In this system the magnetic moments are aligned in the out-of-plane direction of each layer and antialigned in adjacent layers [2,16,18–20]. As a result, monolayer CrI₃ is ferromagnetic [21], bilayer CrI₃ has an antiferromagnetically ordered ground state [18], and bulk CrI₃ is a ferromagnetic semiconductor [11,20,21]. It is noteworthy that the CrCl₃ monolayer displays only an

in-plane magnetic easy axis that dominates over the weak perpendicular magnetocrystalline anisotropy [22]. While all three monolayer components reveal strain-tunable magnetic anisotropy [23], CrI₃ additionally displays pressure [24] and electric field [25] controlled magnetism. With the main absorption peaks lying in the visible part of the spectrum and tunable magnetic properties make the Cr trihalides promising candidates for future magnetoelectronic and magneto-optic devices [26].

It is interesting to note, additionally, that the magnetic ordering temperatures of the Cr trihalides increase as the halogen size increases from Cl to Br to I [6]. Since the Cr-Cr distances increase with increasing halogen size, the superexchange coupling constants between magnetic transition-metal ions [27] are expected to be weakened along this series. Moreover, as the electronegativity is decreased from Cl to I, it has also been argued that the Cr-X bonding becomes more covalent, strengthening superexchange interactions and raising the magnetic ordering temperatures [6].

To address these issues of fundamental and applied importance, including the microscopic origin of intra- and interlayer magnetism, *ab initio* density functional theories (DFT) implemented within the generalized gradient approximation (GGA) and GGA plus Hubbard *U* (GGA + *U*) schemes were performed for CrX₃ systems [11,17,20,21,26,28–30]. These calculations correctly describe the insulating electronic state of the magnetically ordered phases [11,20,31], with almost fully polarized electron bands.

A perusal of extant GGA + *U* studies, which explicitly take into account the effect of intrinsic [10] electron-electron interactions in the Cr 3*d* shell, reveals that the on-site Coulomb interaction *U* for the CrX₃ family could reach values

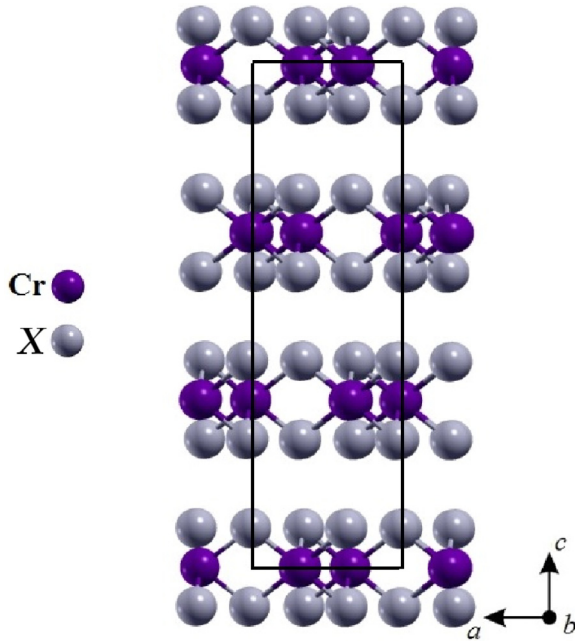


FIG. 1. Schematic representation of the rhombohedral crystal structure of CrX_3 ($X = \text{Br}, \text{Cl}, \text{I}$) crystals. Black lines represent the unit cells.

up to 4.1 eV [17,20,21,28,30]. However, in spite of these theoretical studies of fundamental importance, the dynamical quantum nature of the nonmagnetic electronic state of CrX_3 crystals has been only recently explored [30,31]. Motivated thereby, in this paper we extend our earlier study [31] to perform a detailed comparative analysis for the electronic structure reconstruction of CrX_3 bulk crystals within the GGA plus dynamical mean-field theory (GGA + DMFT) approximation [32], showing how the different chemistry determines the emergent correlated electronic state with distinct orbital-selective many-particle fingerprints. Similar to Refs. [30,31], the current comparative study highlights the importance of incorporating dynamical multiorbital (MO) interaction effects within the Cr $3d$ orbitals to determine the role played by self-energy corrections to the electronic spectra of all three CrX_3 components.

II. RESULTS AND DISCUSSION

The DFT calculations were performed for the paramagnetic electronic state of rhombohedral CrX_3 parent compounds (see Fig. 1) using the SIESTA *ab initio* simulation package [33]. A generalized gradient approximation (GGA) in the Perdew-Burke-Ernzerhof (PBE) implementation [34] was applied as the exchange correlation functional. Norm-conserving pseudopotentials of Troullier-Martins [35] in Kleinman-Bylander nonlocal form were used to represent the ionic core potential. The Kohn-Sham orbitals [36] are expanded in a linear combination of atomic orbitals of finite range which is determined by a common confinement energy shift of 0.01 Ry [37]. The precision of the real-space grid integration is determined by an energy cutoff of 200 Ry [38]. The respective Brillouin zone is sampled by a $10 \times 10 \times 10$ Monkhorst-Pack grid [39] for a primitive cell of bulk CrX_3 .

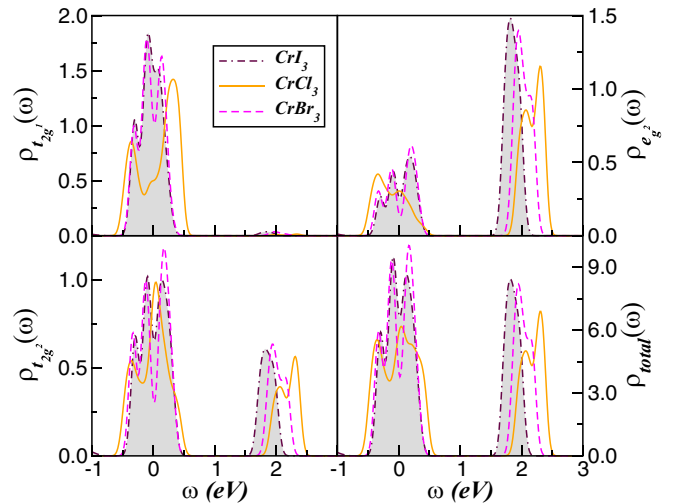


FIG. 2. Effect of chemistry on the bare GGA orbital-resolved and total density of states (DOS) of CrX_3 ($X = \text{I}, \text{Cl}, \text{Br}$) parent compounds, which are composed by twofold degenerate t_{2g}^2 and e_g^2 orbitals and a nondegenerate t_{2g}^1 orbital. Important features to be seen are the narrow bare bandwidth, the changes in the t_{2g} electronic states of CrCl_3 as compared to CrI_3 and CrBr_3 systems, and the fact that all bands in GGA span near the Fermi level, $E_F = \omega = 0$. This latter confirms that the electronic states relevant to chromium trihalides are the Cr $3d$ states.

All the lattice constants were taken from Refs. [8,40]. Finally, as in Ref. [31], the atomic positions were fully optimized until all the force components became smaller than $0.04 \text{ eV}/\text{\AA}$.

To provide insights for the emergent electronic reconstruction due to chemical and electron-electron correlation effects within the rhombohedral structural phase of paramagnetic CrCl_3 and CrBr_3 bulk crystals, we use x-ray absorption spectroscopy (XAS) [41]. As in our earlier study [31], the total fluorescence yield (TFY) mode of XAS spectra was recorded using the qRIXS end station at Beamline 8.0.1 at the Advanced Light Source (ALS), Lawrence Berkeley National Laboratory [42].

To begin with, in Fig. 2 we show the orbital-resolved and total GGA density of states (DOS) of the rhombohedral ($R\bar{3}$) structural phase of paramagnetic CrX_3 bulk crystals. Owing to the octahedral environment of the Cr sites, the $3d$ states split into low-lying t_{2g} and high-lying e_g groups. These two groups are composed by twofold degenerate t_{2g}^2 and e_g^2 orbitals and a nondegenerate t_{2g}^1 orbital [31]. Consistent with earlier DFT studies for the nonmagnetically ordered phase of CrX_3 [11,20], our GGA results in Fig. 2 show that the active electronic states in these Cr-trihalide compounds involve the Cr $3d$ carriers, where all d bands have appreciable weight near the Fermi level, $E_F = \omega = 0$. As common to transition-metal compounds, the e_g^2 states are higher in energy and nearly fully polarized within GGA. However, as shown below, strong MO electron-electron interactions will scatter electrons among different orbital channels via the interorbital Coulomb interaction U' and the Hund's exchange parameter J_H [27], closing the bare band gap between the low-lying t_{2g} and the high in energy e_g^2 states. Also interesting in Fig. 2 is the orbital-selective electronic structure reconstruction induced by the halide ions.

While the electronic states of CrI_3 and CrBr_3 are similar in nature, showing the same bare bandwidth W , pronounced changes are seen with the t_{2g} orbital sector near E_F for the CrCl_3 crystal. Although a one-particle peak emerges at E_F in the t_{2g}^2 DOS, a bonding-antibonding pseudoband gap [11] develops in the electronic state with t_{2g}^1 orbital character due to sizable p - d hybridization in CrCl_3 [10], with the concomitant broadening of the Cr $3d$ band. The chemical changes induced by the halogens in the bare bandwidth W and the electronic line shape near E_F are important one-particle GGA seeds toward the distinct correlated electronic structure reconstruction of the Cr-trihalide bulk crystals, as shown below.

While first-principles calculations have provided reliable information regarding the structural and magnetic ground state properties for CrX_3 crystals [11,17,20–22,28], they are known to generically fail to capture dynamical electron-electron correlation effects [30], and so they cannot access the formation of coherent Kondo quasiparticles and incoherent Hubbard satellites (local moments) at low and high energies [43], respectively. Combining DFT with DMFT is a many-particle prescription for overcoming this problem [32]. Thus, as common to correlated materials within GGA, the one-electron part of the MO Hamiltonian for CrX_3 reads $H_0 = \sum_{\mathbf{k},a,\sigma} \epsilon_a(\mathbf{k}) c_{\mathbf{k},a,\sigma}^\dagger c_{\mathbf{k},a,\sigma} + \sum_{i,a,\sigma} \epsilon_{i,a,\sigma} n_{i,a,\sigma}$, where $a = (t_{2g}^1, t_{2g}^2, e_g^2)$ denotes its diagonalized $3d$ orbitals and $\epsilon_a(\mathbf{k})$ is the corresponding band dispersion, which encodes details of the one-electron band structure. These five Cr $3d$ bands are the relevant one-particle inputs for MO-DMFT which generates a strongly correlated paramagnetic electronic state as shown below. Similar to CrI_3 [31], the $3d$ many-body Hamiltonian relevant for CrX_3 bulk crystals reads $H_{\text{int}} = U \sum_{i,a} n_{i,a,\uparrow} n_{i,a,\downarrow} + U' \sum_{i,a \neq b} n_{i,a} n_{i,b} - J_H \sum_{i,a \neq b} \mathbf{S}_{i,a} \cdot \mathbf{S}_{i,b}$. Here, U is the on-site Coulomb interaction, $U' = U - 2J_H$ is the interorbital Coulomb interaction term, and J_H is the Hund's coupling. To avoid double counting of the (static) mean-field contributions from the electron-electron interactions already included in the DFT [44], the one-particle orbital energies are corrected through their bare GGA values to $\epsilon'_{i,a,\sigma} = \epsilon_{i,a,\sigma} - U(n_{i,a,\sigma} - \frac{1}{2}) + \frac{1}{2}J_H(n_{i,a,\sigma} - 1)$ [45], so that $H'_0 = \sum_{\mathbf{k},a,\sigma} \epsilon_{a,\sigma}(\mathbf{k}) c_{\mathbf{k},a,\sigma}^\dagger c_{\mathbf{k},a,\sigma} + \sum_{i,a,\sigma} \epsilon'_{i,a,\sigma} n_{i,a,\sigma}$. We evaluate the many-particle Green's functions [$G_{\mathbf{k},a,\sigma}(\omega)$] of the correlated many-particle Hamiltonian of CrX_3 bulk crystals within GGA + DMFT [32], using MO iterated perturbation theory (MO-IPT) as the impurity solver [46]. The DMFT solution involves replacing the lattice model by a self-consistently embedded MO-Anderson impurity model, and the self-consistency condition requiring the local impurity Green's function to be equal to the local Green's function for the lattice. The full set of equations for the MO case can be found in Ref. [46] so we do not repeat the equations here. Our real frequency MO-IPT scheme has a proven record of good semiquantitative agreements with experiment for a range of correlated materials, and it gives results for the spectral functions and self-energies in qualitative accord with numerical exact continuous-time quantum Monte Carlo (CT-QMC) calculations [47].

However, before delving into the MO electronic structure reconstruction of CrX_3 bulk crystals, we recall here that the on-site Coulomb interaction parameter is reported to be in the

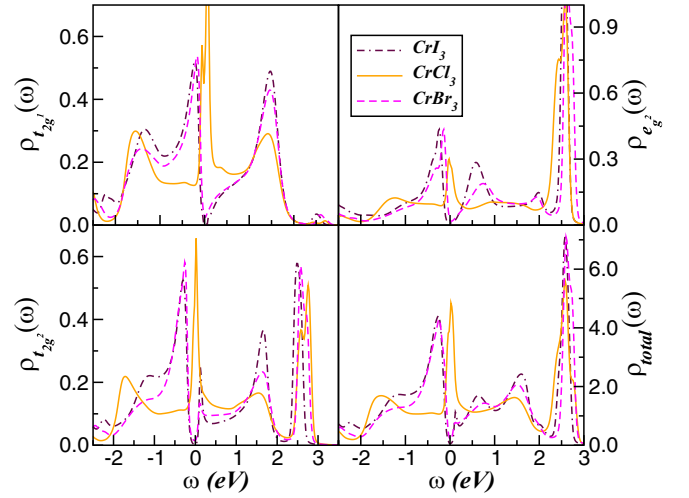


FIG. 3. Comparison between orbital-resolved and total GGA + DMFTDOS for the Cr $3d$ orbitals of rhombohedral CrX_3 bulk crystals, for $U_{t_{2g}^1} = 2.75$ eV, $U_{t_{2g}^2} = U_{e_g^2} = 4.0$ eV, and $J_H = 0.85$ eV. Noteworthy is the electronic reconstruction and the emergence of Kondo quasiparticles (CrCl_3) and Mott localization (CrI_3 and CrBr_3) at low energies, due to strong dynamical transfer of spectral weight within DMFT.

range between 1.0 eV [21] and 4.1 eV [30] for CrI_3 crystals. Thus, given the uncertainty in the precise estimation of U for this layered system [17,20,21,30,44,48] and analogs [49,50] if not mentioned otherwise, we use the U values considered in our earlier GGA + DMFT study [31], i.e., $U_{t_{2g}^1} = 2.75$ eV and $U_{t_{2g}^2} = U_{e_g^2} = 4.0$ eV, and fixed $J_H = 0.85$ eV [20], where good theory-experiment agreement has been found within the paramagnetic phase of CrI_3 bulk crystal.

With this in place, let us now turn our attention to the GGA + DMFT (MO-IPT) results obtained within the formal Cr^{3+} oxidation state of the CrX_3 parent compounds. In Fig. 3 we display the combined effect of chemistry and MO dynamical correlations on the orbital-resolved and total [$\rho_{\text{total}}(\omega) = \sum_{a,\sigma} \rho_{a,\sigma}(\omega)$] [51] spectral functions of rhombohedral CrX_3 bulk crystals. As seen at fixed $U_{t_{2g}^1} = 2.75$ eV and $U_{t_{2g}^2} = U_{e_g^2} = 4.0$ eV values the CrI_3 and CrBr_3 systems are paramagnetic Mott insulators, where all orbitals display a Mott-Hubbard gap at E_F [52]. In spite of the orbital-selective transfer of spectral weight, lower (LHB) and upper (UHB) Hubbard bands at high energies are visible in a more or less pronounced way, depending on the orbital character, in all orbital-resolved spectral functions. This behavior highlights the intrinsic tendency toward a large transfer of spectral weight in transition-metal compounds [52], where the U/W ratio is sizable [10]. Moreover, as seen in Fig. 3, paramagnetic CrCl_3 is in the Kondo-metallic state [43], showing narrow Kondo quasiparticles at low energies followed by incoherent Hubbard bands relevant for the local moment (LHBs) formation in CrCl_3 . Interestingly, similar Kondo-lattice behavior with a peak-deep-hump line shape as in Fig. 3 has been observed for Fe_3GeTe_2 [53], suggesting a possible common underlying Kondo scenario for itinerant van der Waals crystals.

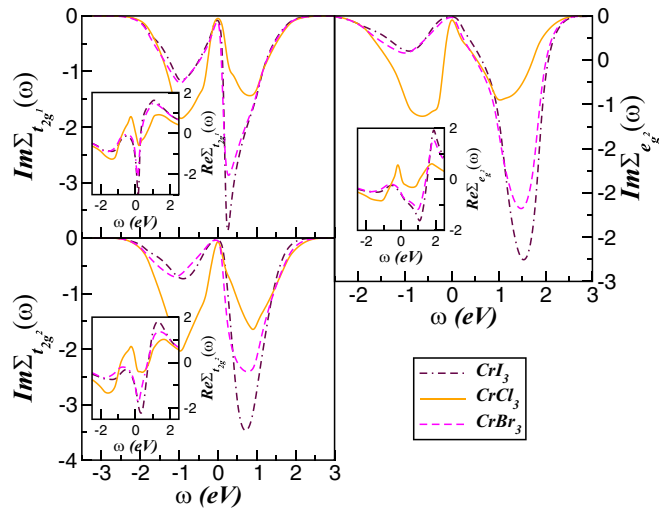


FIG. 4. Orbital-resolved self-energy imaginary (main panels) and real (insets) parts of CrX_3 bulk crystals, showing their chemical evolution for fixed $U_{t_{2g}^1} = 2.75$ eV, $U_{t_{2g}^2} = U_{e_g} = 4.0$ eV, and $J_H = 0.85$ eV values. A particular feature to be seen is the clearly visible particle-hole asymmetry and the strong frequency dependence of the self-energy real parts within the Mott localized CrI_3 and CrBr_3 systems.

Additionally, in Fig. 4, we show the chemical dependence of the self-energy imaginary (main panels) and real (insets) parts associated with the active $3d$ orbitals of CrX_3 bulk crystals. Comparing our results to that reported, for example, for the body-centered-tetragonal (bct) phase of NbO_2 [54] or that recently reported for LaCoO_3 [55], we notice similar features in these different transition-metal systems, i.e., the absence of poles at E_F and the strong particle-hole asymmetry in $\Sigma_a(\omega)$. This particle-hole asymmetry is manifested by the appearance of a peak above E_F in $\text{Im}\Sigma_a(\omega)$, which becomes almost particle-hole symmetric in the Kondo-metallic phase of CrCl_3 . Taking together our results and those obtained using DFT plus cluster-DMFT calculations [54], a remarkable aspect stands out: $\text{Im}\Sigma_a(\omega)$ vanishes in the region of the Mott gap, instead of having a pole, as would occur in a conventional Mott insulator. Importantly, as can be seen in the insets of Fig. 4, the self-energy real parts of the Mott localized components have a pronounced frequency dependence near E_F , which indicates that the bare electronic states are strongly renormalized by the orbital-resolved self-energy real parts, stabilizing the Mott insulating state as in bct NbO_2 [54].

A plausible reason why CrCl_3 is not Mott localized as compared to the other two CrX_3 components might be related with the deep in the t_{2g}^1 DOS in GGA as well as the bare $t_{2g}-e_g$ band broadening, which in turn reduces the effective U/W ratio in GGA + DMFT. Thus, it seems that the most natural way to induce Mott localization in CrCl_3 is to increase the on-site Coulomb interaction U , particularly within the t_{2g}^1 orbital sector. It is worth mentioning here, however, that Refs. [10,30] give an estimate of $U \simeq 4.0$ eV for Cr in CrI_3 . With this in place, in Fig. 5 we display the effect of electron-electron interactions in the orbital-selective and the total spectral function of CrCl_3 . As seen, up to $U_1 = 4.0$ eV paramagnetic CrCl_3 remains in the Kondo-metallic side of

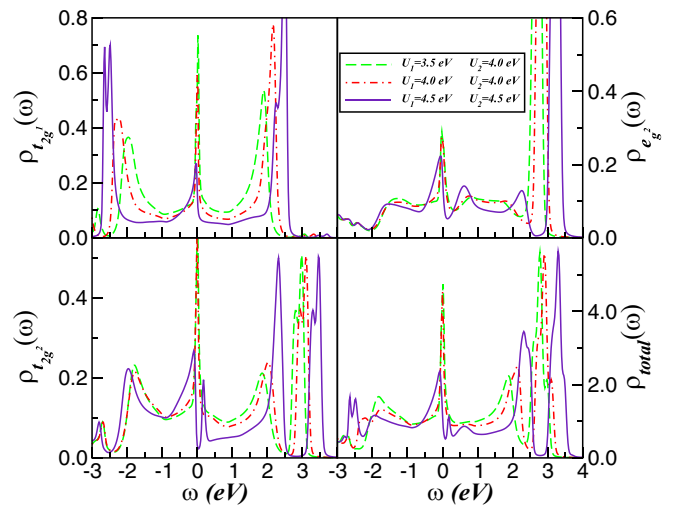


FIG. 5. Effect of multiorbital electron-electron interactions in the orbital-resolved and total DOS of CrCl_3 bulk crystal, showing their evolution towards orbital selectivity. Notice the suppression of the Kondo-quasiparticle resonances and the emergence of pseudogapped electronic localization in the double-degenerate orbital of CrCl_3 at low energies for $U_1 = U_2 = 4.5$ eV.

the correlated phase diagram [52]. However, upon increasing the on-site U ($\equiv U_1 = U_2 = 4.5$ eV), the Kondo-quasiparticle peak in the t_{2g}^1 orbital is strongly depleted and a pseudogapped electronic state emerges in the two double-degenerate $t_{2g}-e_g$ channels. Thus, according to our GGA + DMFT results, the Mott-Hubbard insulating state of rhombohedral CrCl_3 might possibly be tuned in strained crystals [23], where larger effective U values can be achieved via strain inducing one-particle band narrowing. We leave this problem for future studies.

Finally, in Fig. 6, we compare the XAS spectrum obtained at 100 K for the rhombohedral structural phase of CrCl_3 and CrBr_3 bulk crystals with the deconvoluted GGA + DMFT DOS of Fig. 3 using a Lorentzian broadening of 0.35 eV in order to include experimental resolution and lifetime effects [31,56]. Interestingly and consistent with the total GGA + DMFT spectral functions in Fig. 3, the XAS data show electronic structure reconstruction over the entire energy range (see the inset of Fig. 6), implying that the resonant absorption processes probed by XAS are sensitive to the chemical and electronic structure details. Remarkably, our theory-experiment comparison for the Mott localized electronic state of CrBr_3 bulk crystal is consistent with an earlier DFT + DMFT study on the Mott transition in V_2O_3 [57], demonstrating that the structure of the core-hole potential in the K edge spectroscopy allows us to associate the pre-edge spectrum with the k -integrated spectral function above the Fermi energy calculated using the DFT + DMFT approximation. As visible in the main panel of Fig. 6, the incoherent part of the GGA + DMFT spectral function and the experimental spectrum of CrBr_3 bulk crystal agree in many aspects, especially as for the splitting of the first two peaks. This validates the choice of the Coulomb parameter values used in our calculations [31], contrasting with values assumed in previous studies [17,20,21,28,30,48,49]. However, while good

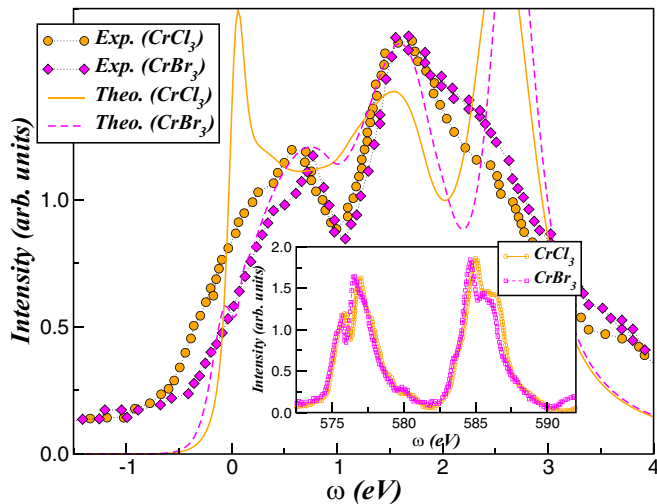


FIG. 6. Comparison between experimental XAS spectrum and GGA + DMFT results for $U_{t_{2g^1}} = 2.75$ eV, $U_{t_{2g^2}} = U_{e_g^2} = 4.0$ eV, and $J_H = 0.85$ eV within the rhombohedral structural phase of paramagnetic CrCl_3 and CrBr_3 bulk crystals, showing qualitatively good theory-experiment agreement up to 1.6 eV above E_F for CrBr_3 . (The inset shows the XAS spectra in a larger energy window.) The theoretical curves are broadened by a Lorentzian in order to include experimental resolution and lifetime effects. In the main panel the XAS data for CrCl_3 were shifted downwards by 0.35 eV to show its broad low-energy line shape as compared to CrBr_3 bulk crystal, a fingerprint of low-energy electronic excitations partially probed in experiment.

theory-experiment agreement is obtained at low energies for CrBr_3 , noticeable differences are seen in the case CrCl_3 bulk crystal. We shall notice here that due to core-hole lifetime effects [56], or the interaction of the $3d$ states with the core-hole [56], the pre-edge features of the experimental XAS spectra are known to be related with the incoherent part of the correlated spectral function [57]. The physical reason is that the core-hole potential, which is an important parameter to correctly describe the near-edge absorption spectra of metals [56], induces electronic localization, destroying the coherent Kondo-quasiparticle excitations. Thus, in view of the

fact that the XAS spectrum is localized at low energies, no sharp resonance feature near E_F is observed in the unoccupied XAS spectra at low energies as in Fig. 6. Future combined photoemission (PES) and bremsstrahlung isochromat (BIS) studies [58] are called for to resolve the low-energy, correlated electronic structure of rhombohedral CrCl_3 bulk crystal.

III. CONCLUSION

In summary, in this work we have performed a comparative GGA and GGA + DMFT study for the electronic structure reconstruction in the Cr-trihalide parent compounds. Using a realistic local Coulomb interaction in the multi-orbital Hubbard model, we provide a microscopic description of the excitation spectrum which emerges within the paramagnetic, nonmagnetically ordered state of the rhombohedral CrX_3 ($X = \text{I}, \text{Cl}, \text{Br}$) bulk series. While the true nature of the Mott insulating state of CrCl_3 remains to be seen, the central message of our approach is to show that a strong coupling [10] picture leads to a satisfying description for the insulating gap of CrBr_3 , showing similar multi-orbital electronic structure reconstruction as for CrI_3 [31]. Taken together, our comparative analysis provides support for the dynamical electronic structure reconstruction in CrX_3 parent compounds [30], and it is expected to be generally applicable to understanding orbital selectivity in strongly interacting electron systems and the underlying electronic state which might emerge in van der Waals magnetic materials [59].

ACKNOWLEDGMENTS

L.C.'s work is supported by CNPq (Grant No. 304035/2017-3). L.C. thanks Jörg Fink for useful discussions. Acknowledgement (L.C. and S.S.C.) is also made to CAPES. The experimental research used resources of the Advanced Light Source, a US DOE Office of Science User Facility under Contract No. DE-AC02-05CH11231. The work in Houston was supported in part by the State of Texas through the Texas Center for Superconductivity at the University of Houston.

- [1] H. H. Kim, B. Yang, S. Li, S. Jiang, C. Jin, Z. Tao, G. Nichols, F. Sfigakis, S. Zhong, C. Li, S. Tian, D. G. Cory, G.-X. Miao, J. Shane, K. F. Mak, H. Lei, K. Sun, L. Zhao, and A. W. Tsien, *Proc. Natl. Acad. Sci. USA* **116**, 11131 (2019).
- [2] Z. Wang, I. Gutiérrez-Lezama, N. Ubrig, M. Kroner, M. Gibertini, T. Taniguchi, K. Watanabe, A. Imamoğlu, E. Giannini, and A. F. Morpurgo, *Nat. Commun.* **9**, 2516 (2018); D. Zhong, K. L. Seyler, X. Linpeng, N. P. Wilson, T. Taniguchi, K. Watanabe, M. A. McGuire, K.-M. C. Fu, D. Xiao, W. Yao, and X. Xu, *Nat. Nanotechnol.* **15**, 187 (2020).
- [3] Z. Wang, M. Gibertini, D. Dumcenco, T. Taniguchi, K. Watanabe, E. Giannini, and A. F. Morpurgo, *Nat. Nanotechnol.* **14**, 1116 (2019); D. R. Klein, D. MacNeill, Q. Song, D. T. Larson, S. Fang, M. Xu, R. A. Ribeiro, P. C. Canfield, E. Kaxiras, R. Comin, and P. Jarillo-Herrero, *Nat. Phys.* **15**, 1255 (2019).
- [4] M. Kim, P. Kumaravadivel, J. Birkbeck, W. Kuang, S. G. Xu, D. G. Hopkinson, J. Knolle, P. A. McClarty, A. I. Berdyugin, M. Ben Shalom, R. V. Gorbachev, S. J. Haigh, S. Liu, J. H. Edgar, K. S. Novoselov, I. V. Grigorieva, and A. K. Geim, *Nat. Electron.* **2**, 457 (2019); C. Jin, Z. Tao, K. Kang, K. Watanabe, T. Taniguchi, K. F. Mak, and J. Shan, *Nat. Mater.* **19**, 1290 (2020).
- [5] M. A. McGuire, H. Dixit, V. R. Cooper, and B. C. Sales, *Chem. Mater.* **27**, 612 (2015).
- [6] M. A. McGuire, G. Clark, Santosh KC, W. M. Chance, G. E. Jellison, Jr., V. R. Cooper, X. Xu, and B. C. Sales, *Phys. Rev. Materials* **1**, 014001 (2017).
- [7] L. L. Handy and N. W. J. Gregory, *J. Am. Chem. Soc.* **74**, 891 (1952); B. Morosin and J. Narath, *J. Chem. Phys.* **40**, 1958 (1964).
- [8] I. Tsubokawa, *J. Phys. Soc. Jpn.* **15**, 1664 (1960).

- [9] J. W. Cable, M. K. Wilkinson, and E. O. Wollan, *J. Phys. Chem. Solids* **19**, 29 (1961).
- [10] I. Pollini, *Phys. Rev. B* **50**, 2095 (1994).
- [11] H. Wang, V. Eyert, and U. Schwingenschlöggl, *J. Phys.: Condens. Matter* **23**, 116003 (2011).
- [12] J. Zeisner, K. Mehawat, A. Alfonsov, M. Roslova, T. Doert, A. Isaeva, B. Büchner, and V. Kataev, *Phys. Rev. Materials* **4**, 064406 (2020).
- [13] D. Soriano, M. I. Katsnelson, and J. Fernández-Rossier, *Nano Lett.* **20**, 6225 (2020).
- [14] See also, A. S. Ahmad, Y. Liang, M. Dong, X. Zhou, L. Fang, Y. Xia, J. Dai, X. Yan, X. Yu, G. Zhang, Y. Zhao, and S. Wang, *Nanoscale* **12**, 22935 (2020).
- [15] C. Gong and X. Zhang, *Science* **363**, 706 (2019).
- [16] H. Li, S. Ruan, and Y.-J. Zeng, *Adv. Mater.* **31**, 1900065 (2019).
- [17] P. Jiang, C. Wang, D. Chen, Z. Zhong, Z. Yuan, Z.-Y. Lu, and W. Ji, *Phys. Rev. B* **99**, 144401 (2019).
- [18] Z. Sun, Y. Yi, T. Song, G. Clark, B. Huang, Y. Shan, S. Wu, D. Huang, C. Gao, Z. Chen, M. McGuire, T. Cao, D. Xiao, W.-T. Liu, W. Yao, X. Xu, and S. Wu, *Nature (London)* **572**, 497 (2019).
- [19] B. Huang, G. Clark, E. Navarro-Moratalla, D. R. Klein, R. Cheng, K. L. Seyler, D. Zhong, E. Schmidgall, M. A. McGuire, D. H. Cobden, W. Yao, D. Xiao, P. Jarillo-Herrero, and X. Xu, *Nature (London)* **546**, 270 (2017); T. Song, X. Cai, M. W.-Y. Tu, X. Zhang, B. Huang, N. P. Wilson, K. L. Seyler, L. Zhu, T. Taniguchi, K. Watanabe, M. A. McGuire, D. H. Cobden, D. Xiao, W. Yao, and X. Xu, *Science* **360**, 1214 (2018).
- [20] O. Besbes, S. Nikolaev, N. Meskini, and I. Solov'yev, *Phys. Rev. B* **99**, 104432 (2019).
- [21] V. K. Gudelli and G.-Y. Guo, *New J. Phys.* **21**, 053012 (2019).
- [22] F. Xue, Y. Hou, Z. Wang, and R. Wu, *Phys. Rev. B* **100**, 224429 (2019).
- [23] L. Webster and J.-A. Yan, *Phys. Rev. B* **98**, 144411 (2018).
- [24] T. Li, S. Jiang, N. Sivasdas, Z. Wang, Y. Xu, D. Weber, J. E. Goldberger, K. Watanabe, T. Taniguchi, C. J. Fennie, K. F. Mak, and J. Shan, *Nat. Mater.* **18**, 1303 (2019).
- [25] S. Jiang, L. Li, Z. Wang, K. F. Mak, and J. Shan, *Nat. Nanotechnol.* **13**, 549 (2018).
- [26] W.-B. Zhang, Q. Qu, P. Zhu, and C.-H. Lam, *J. Mater. Chem. C* **3**, 12457 (2015).
- [27] S. Feldkemper and W. Weber, *Phys. Rev. B* **57**, 7755 (1998).
- [28] J. L. Lado and J. Fernández-Rossier, *2D Mater.* **4**, 035002 (2017).
- [29] M. Pizzochero, R. Yadav, and O. V. Yazyev, *2D Mater.* **7**, 035005 (2020).
- [30] Y. O. Kvashnin, A. N. Rudenko, P. Thunström, M. Rösner, and M. I. Katsnelson, *arXiv:2012.13562*.
- [31] L. Craco, S. S. Carara, Y.-C. Shao, Y.-D. Chuang, and B. Freelon, *Phys. Rev. B* **102**, 195130 (2020).
- [32] G. Kotliar, S. Y. Savrasov, K. Haule, V. S. Oudovenko, O. Parcollet, and C. A. Marianetti, *Rev. Mod. Phys.* **78**, 865 (2006).
- [33] J. M. Soler, E. Artacho, J. D. Gale, A. García, J. Junquera, P. Ordejón, and D. Sánchez-Portal, *J. Phys.: Condens. Matter* **14**, 2745 (2002); E. Artacho, E. Anglada, O. Dieguez, J. D. Gale, A. García, J. Junquera, M. Martín, P. Ordejón, J. M. Pruneda, D. Sánchez-Portal, and J. M. Soler, *ibid.* **20**, 064208 (2008).
- [34] J. P. Perdew, K. Burke, and M. Ernzerhof, *Phys. Rev. Lett.* **77**, 3865 (1996).
- [35] N. Troullier and J. L. Martins, *Phys. Rev. B* **43**, 1993 (1991).
- [36] W. Kohn and L. J. Sham, *Phys. Rev.* **140**, A1133 (1965).
- [37] J. Junquera, Ó. Paz, D. Sánchez-Portal, and E. Artacho, *Phys. Rev. B* **64**, 235111 (2001).
- [38] J. Moreno and J. M. Soler, *Phys. Rev. B* **45**, 13891 (1992).
- [39] H. J. Monkhorst and J. D. Pack, *Phys. Rev. B* **13**, 5188 (1976).
- [40] S. Djurdjic-Mijin, A. Šolajić, J. Pešić, M. Šćepanović, Y. Liu, A. Baum, C. Petrovic, N. Lazarević, and Z. V. Popović, *Phys. Rev. B* **98**, 104307 (2018).
- [41] Y. C. Shao, B. Karki, W. Huang, X. Feng, G. Sumanasekera, J.-H. Guo, Y.-D. Chuang, and B. Freelon, *J. Phys. Chem. Lett.* **12**, 724 (2021).
- [42] Y.-D. Chuang, X. Feng, A. Cruz, K. Hanzel, A. Brown, A. Spucce, A. Frano, W.-S. Lee, J. Kim, Y.-J. Chen, B. Smith, J. S. Pepper, Y.-C. Shao, S.-W. Huang, L. A. Wray, E. Gullikson, Z.-X. Shen, T. P. Devereaux, A. Tremis, W. Yang *et al.*, *J. Electron Spectrosc. Relat. Phenom.*, (2019), doi: 10.1016/j.elspec.2019.146897.
- [43] A. Georges, G. Kotliar, W. Krauth, and M. J. Rozenberg, *Rev. Mod. Phys.* **68**, 13 (1996).
- [44] S. Sarkar and P. Kratzer, *Phys. Rev. Materials* **4**, 104006 (2020).
- [45] L. Craco, M. S. Laad, and E. Müller-Hartmann, *Phys. Rev. Lett.* **90**, 237203 (2003).
- [46] L. Craco, *Phys. Rev. B* **77**, 125122 (2008).
- [47] L. Craco and S. Leoni, *Phys. Rev. B* **100**, 121101(R) (2019); **102**, 045142 (2020).
- [48] D. Soriano, A. N. Rudenko, M. I. Katsnelson, and M. Rösner, *arXiv:2103.04686*.
- [49] D. L. Esteras and J. J. Baldoví, *arXiv:2104.03023*.
- [50] I. Pollini, *Solid State Commun.* **113**, 559 (2000).
- [51] $\rho_{a,\sigma}(\omega) \equiv -\frac{1}{\pi} \sum_{\mathbf{k}} G_{a,\sigma}(\mathbf{k}, \omega)$, with $G_{a,\sigma}(\mathbf{k}, \omega) = \frac{1}{\omega + \mu - \sum_{a,\sigma} \epsilon_a(\mathbf{k})}$ being the retarded one-particle Green's function of orbital a .
- [52] M. Imada, A. Fujimori, and Y. Tokura, *Rev. Mod. Phys.* **70**, 1039 (1998).
- [53] Y. Zhang, H. Lu, X. Zhu, S. Tan, W. Feng, Q. Liu, W. Zhang, Q. Chen, Y. Liu, X. Luo, D. Xie, L. Luo, Z. Zhang, and X. Lai, *Sci. Adv.* **4**, eaa06791 (2018).
- [54] W. H. Brito, M. C. O. Aguiar, K. Haule, and G. Kotliar, *Phys. Rev. B* **96**, 195102 (2017).
- [55] H. Park, R. Nanguneri, and A. T. Ngo, *Phys. Rev. B* **101**, 195125 (2020).
- [56] J. Fink, T. Müller-Heinzerling, B. Scheerer, W. Speier, F. U. Hillebrecht, J. C. Fuggle, J. Zaanen, and G. A. Sawatzky, *Phys. Rev. B* **32**, 4899 (1985).
- [57] F. Rodolakis, P. Hansmann, J.-P. Rueff, A. Toschi, M. W. Haverkort, G. Sangiovanni, A. Tanaka, T. Saha-Dasgupta, O. K. Andersen, K. Held, M. Sikora, I. Alliot, J.-P. Itié, F. Baudelet, P. Wzietek, P. Metcalf, and M. Marsi, *Phys. Rev. Lett.* **104**, 047401 (2010).
- [58] M. Matsunami, M. Taguchi, A. Chainani, R. Eguchi, M. Oura, A. Sakai, S. Nakatsuji, and S. Shin, *Phys. Rev. B* **84**, 193101 (2011).
- [59] K. F. Mak, J. Shan, and D. C. Ralph, *Nat. Rev. Phys.* **1**, 46 (2019); M. Gibertini, M. Koperski, A. F. Morpurgo, and K. S. Novoselov, *Nat. Nanotechnol.* **14**, 408 (2019); S. O. Valenzuela and S. Roche, *ibid.* **14**, 1088 (2019).